6th European Conference on Computational Mechanics (ECCM 6)
7th European Conference on Computational Fluid Dynamics (ECFD 7)
1115 June 2018, Glasgow, UK

SOLID-SHELLS BASED ON REDUCED INTEGRATION - GEOMETRICALLY NON-LINEAR ANALYSIS OF LAYERED STRUCTURES

O. Barfusz[1], R. Smeenk[2] and S. Reese[1]

[1] Institute of Applied Mechanics, RWTH Aachen University, D-52074 Aachen, Germany,
{oliver.barfusz, stefanie.reese}@rwth-aachen.de
[2] Eindhoven University of Technology, De Rondom 70, 5612 AP Eindhoven, Netherlands
r.m.a.smeenk@student.tue.nl

Key words: Solid-shell, reduced integration, hourglass stabilization, anisotropy

Abstract. Some years ago, a family of solid-shell finite elements based on reduced integration [1],[2],[3],[4] was investigated. Many engineering problems with isotropic material behaviour were considered and these elements showed accurate results while beeing more efficient than similar three-dimensional formulations based on full integration. The objective of the present contribution is the extension to layered structures with anisotropic material behaviour undergoing large deformations. Here, we follow an ansatz which is similar to so called equivalent single layer theories, i.e. we model the inhomogeneous material as a continuum using solely one solid-shell element over the thickness. Therefore, some modifications of the element formulation are needed. First, we introduce an additional mapping procedure which enables both, the usage of a certain quadrature rule within each layer of the composite and the consideration of layers with different thicknesses. Second, we investigate an appropriate hourglass-stabilization which is needed to recover so-called zero energy modes which might arise from the reduced integration scheme. Considering a benchmark problem from the literature, it will be shown that the new developed ingredients within the solid-shell concept lead to accurate results in terms of the global response of anisotropic structures at large deformations.

1 INTRODUCTION

For future space transportation systems, investigations encompassing higher payloads and further performance increases always play an important role. In order to decrease the dependence of the design process on experimental test campaigns, reliable simulation tools have to be developed to be able to predict the mechanical behaviour of rocket engine nozzle structures. In addition to the research on conventional nozzle structures made out of heavy metal super alloys, e.g. [5], composite materials are very promising in lightweight constructions due to their very high stiffness and low density at the same time. They are built up of multiple layers each of which consists of fibres embedded in a matrix material. In aerospace engineering one can find ceramics which can be used for both fibres and

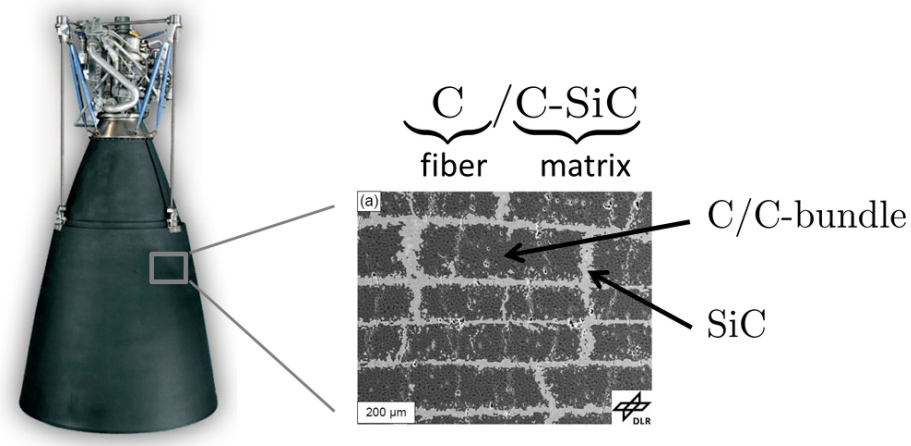

Figure 1: Vinci rocket engine with corresponding microstructure of the CMC material [6]

matrices, see e.g. Fig. 1. Due to different damage mechanisms like matrix cracking, delamination and fibre pullout, the stress-strain behaviour of ceramic matrix composites (CMC) is non-linear and strongly depends on the fibre direction. Moreover, the material's response in tension and compression may differ significantly. In the present contribution we use a modified version of the micromechanically motivated model proposed in [7, 8]. Therein, an anisotropic model has been presented for the hyperelastic material behaviour of pneumatic membranes reinforced with woven fibres which is particularly suitable for the considered CMC material. In order to overcome locking phenomena, the discretization of thin nozzle structures requires an appropriate finite element technology. For this reason we use a solid-shell finite element formulation based on reduced integration [3], for which the implementation of the fibre orientation is crucial.

2 ANISOTROPIC CONSTITUTIVE MODEL

2.1 Continuum mechanical framework

Introducing the deformation gradient $\mathbf{F}$, the deformation of a continuous body is represented by the right Cauchy-Green tensor $\mathbf{C} = \mathbf{F}^T\mathbf{F}$. Using the concept of hyperelasticity, the strain energy density function (SEDF) $\psi = \psi(\mathbf{C})$ is defined as a scalar potential. In the anisotropic case considered here, the energy function $\psi = \psi(\mathbf{C}, \mathbf{M}_i)$ is a scalar function of $\mathbf{C}$ and the structural tensors $\mathbf{M}_i$, which are defined as $\mathbf{M}_i = \mathbf{n}_i \otimes \mathbf{n}_i$, where the unit vectors $\mathbf{n}_i$ are oriented parallel to the fibres. Obviously, for unidirectional layers, only one vector $\mathbf{n}$ and one structural tensor $\mathbf{M} = \mathbf{n} \otimes \mathbf{n}$ need to be defined, where for woven composites with two families of fibres, two vectors $\mathbf{n}_1$ and $\mathbf{n}_2$ are used leading to the structural tensors $\mathbf{M}_1 = \mathbf{n}_1 \otimes \mathbf{n}_1$ and $\mathbf{M}_2 = \mathbf{n}_2 \otimes \mathbf{n}_2$. Then, the SEDF can be represented in dependence of the three principal invariants of $\mathbf{C}$

$$I_1 = \operatorname{tr} \mathbf{C} \qquad I_2 = \frac{1}{2}\left[(\operatorname{tr} \mathbf{C})^2 - \operatorname{tr}\left(\mathbf{C}^2\right)\right] \qquad I_3 = \det \mathbf{C} \tag{1}$$

and the following mixed invariants

$$\begin{aligned} I_4 &= \mathrm{tr}\,(\mathbf{C}\,\mathbf{M}_1) = \mathbf{C}\cdot\mathbf{M}_1 & \qquad I_5 &= \mathrm{tr}\left(\mathbf{C}^2\,\mathbf{M}_1\right) = \mathbf{C}^2\cdot\mathbf{M}_1 \\ I_6 &= \mathrm{tr}\,(\mathbf{C}\,\mathbf{M}_2) = \mathbf{C}\cdot\mathbf{M}_2 & \qquad I_7 &= \mathrm{tr}\left(\mathbf{C}^2\,\mathbf{M}_2\right) = \mathbf{C}^2\cdot\mathbf{M}_2 \end{aligned} \tag{2}$$

The inner product of $\mathbf{C}$ and $\mathbf{M}_i$ $(i = 1, 2)$ can be interpreted as a weighted stretch in the direction of the corresponding structural vector. The anisotropy is taken into account within the scalar SEDF by adding terms that depend on additional invariants. In this work, a SEDF is proposed based on the following formulation by [7]

$$\psi = \psi_{NH}(I_1, I_3) + \psi_{iso}(I_1, I_2) + \psi_{ani}(I_1, I_4, I_5, I_6, I_7), \tag{3}$$

where ψ_{NH} denotes a Neo-Hookean part, ψ_{iso} an additional isotropic part which is needed to model the extreme stiffening in the large strain case, and ψ_{ani} is the anisotropic part referring to the fibre direction. This SEDF has been originally proposed for a rubber-like matrix material reinforced with polyester fibres. To adjust it to the CMC considered here, some modifications are necessary. First of all, the CMC consists of unidirectional plies each of which consists of a carbon fibre reinforced carbon matrix surrounded by a silicon carbide matrix (C/C-SiC), cf. Fig. 1. Therefore, we will restrict our constitutive model to transversely isotropic material behaviour. Secondly, in the original formulation the fibres were assumed to carry no load at all under compression. Due to the continuous support of the fibres, this assumption is not realistic for the CMC considered here. And third, the Neo-Hookean part ψ_{NH} can be neglected, because the isotropic response can be adequately described by the part ψ_{iso} in the moderate strain regime, which is defined as

$$\psi_{iso} = K_1^{iso}(I_1 - 3)^{\alpha_1} + K_2^{iso}(I_2 - 3)^{\alpha_2}. \tag{4}$$

The anisotropic part for a transversely isotropic material can be described by

$$\psi_{ani} = K_1^{ani}\,(I_4 - 1)^{\beta_1} + K_2^{ani}\,(I_5 - 1)^{\beta_2} + K^c\,(I_1 - 3)^{\delta}(I_4 - 1)^{\delta}\,. \tag{5}$$

The resulting SEDF for unidirectional materials reads

$$\begin{aligned} \psi \;=& K_1^{iso}(I_1 - 3)^{\alpha_1} + K_2^{iso}(I_2 - 3)^{\alpha_2} \\ &+ K_1^{ani}\,(I_4 - 1)^{\beta_1} + K_2^{ani}\,(I_5 - 1)^{\beta_2} + K^c\,(I_1 - 3)^{\delta}(I_4 - 1)^{\delta}\,. \end{aligned} \tag{6}$$

The nonlinear model contains the following ten material parameters K_1^{iso}, K_2^{iso}, K_1^{ani}, K_2^{ani}, K^c, α_1, α_2, β_1, β_2 and δ, which have to be fitted to experimental data. The second Piola-Kirchhoff stress tensor $\boldsymbol{S}$ is determined from

$$\boldsymbol{S} = 2\frac{\partial\psi}{\partial\boldsymbol{C}} = 2\frac{\partial\psi}{\partial I_\alpha}\frac{\partial I_\alpha}{\partial\boldsymbol{C}}\,, \tag{7}$$

where $\alpha = 1, \ldots, 5$. The corresponding fourth-order material tensor $\boldsymbol{\mathcal{C}}$ is defined as

$$\boldsymbol{\mathcal{C}} = 4\frac{\partial^2\psi}{\partial\boldsymbol{C}\,\partial\boldsymbol{C}} = 2\frac{\partial\boldsymbol{S}}{\partial\boldsymbol{C}}\,. \tag{8}$$

2.2 Modified strain energy function and material parameters

In order to further simplify the model of section 2.1 we require $\boldsymbol{S}$ to be linear in $\boldsymbol{C}$. To achieve this, the exponents of the nonlinear model (6) are set to

$$\alpha_1 = 2, \quad \alpha_2 = 1, \quad \beta_1 = 2, \quad \beta_2 = 1, \quad \delta = 1 \tag{9}$$

In order to obtain a stress-free undeformed state, the terms

$$\Delta\psi_{iso} = -2K_2^{iso}(I_1 - 3) \qquad \Delta\psi_{ani} = -2K_2^{ani}(I_4 - 1) \tag{10}$$

have to be added to the SEDF. The resulting modified SEDF for unidirectional materials reads

$$\begin{aligned} \psi_{ud} =& K_1^{iso}(I_1 - 3)^2 + K_2^{iso}\left[(I_2 - 3) - 2(I_1 - 3)\right] \\ &+ K_1^{ani}(I_4 - 1)^2 + K_2^{ani}\left[(I_5 - 1) - 2(I_4 - 1)\right] + K^c(I_1 - 3)(I_4 - 1)\,. \end{aligned} \tag{11}$$

This St.Venant-Kirchhoff type model contains the five material parameters K_1^{iso}, K_2^{iso}, K_1^{ani}, K_2^{ani} and K^c. In order to determine those, the constant material tensor in Voigt notation $\hat{\boldsymbol{\mathcal{C}}}_{ud}$ of the modified model with fibre direction $\boldsymbol{n}^T = (1, 0, 0)$ is compared to the well known stiffness matrix for transversely isotropic materials, containing the engineering constants, i.e. Young's moduli, shear moduli and Poisson's ratios. As a result of this comparison, the following relations can be obtained:

$$\begin{aligned} K_1^{iso} &= \frac{E_2\nu_{23} + 2G_{23}v + E_2\nu_{12}\nu_{21} + 2G_{23}v\nu_{23}}{8v(\nu_{23} + 1)} \\ K_2^{iso} &= -\frac{1}{2}G_{23} \\ K_1^{ani} &= \frac{E_1(1 - 2\nu_{21} - 2\nu_{21}\nu_{23} - \nu_{23}^2) + E_2(\nu_{23} + \nu_{12}\nu_{21})}{8v(\nu_{23} + 1)} + \frac{1}{4}(G_{23} - 2G_{12}) \\ K_2^{ani} &= \frac{1}{2}(G_{12} - G_{23}) \\ K^c &= \frac{E_1\nu_{21} - E_2\nu_{23} - E_2\nu_{12}\nu_{21} + E_1\nu_{21}\nu_{23}}{4v(\nu_{23} + 1)}. \end{aligned} \tag{12}$$

with $v = 1 - \nu_{23} - 2\nu_{12}\nu_{21}$, $\nu_{21} = \frac{E_2}{E_1}\nu_{12}$ and $\nu_{23} = \frac{E_2}{2G_{23}} - 1$. Therewith, the five material parameters of the proposed model can be uniquely determined from the five engineering constants of the transversely isotropic effective material. Furthermore this model automatically fulfils the principle of material frame-indifference and can be easily extended to the large strain regime.

3 FE technology

As already mentioned in chapter 1 we use sophisticated solid-shell finite elements based on the works by [2, 3], for the discretization of the considered composite structures. In order to overcome different kinds of locking phenomena, a tailored combination of the

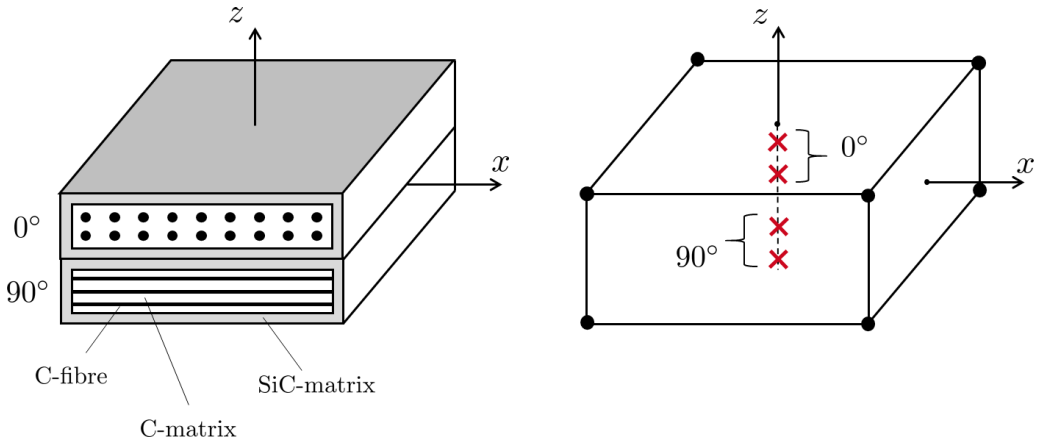

Figure 2: (left) C/C-SiC sample geometry with two layers [0°/90°]; (right) model generation of C/C-SiC using one solid-shell element with multiple integration points over the thickness

enhanced assumed strain (EAS) method and the assumed natural strain (ANS) method is utilized. Furthermore, we use reduced integration with hourglass stabilization in order to increase numerical efficiency as well as the robustness for distorted element geometries. Here we avoid the repetition of the element formulation and refer to [3] for further details. Instead, we focus on the two newly developed ingredients within the solid-shell concept, which have to be considered in order to investigate layered structures.

3.1 Extension to layered structures - thickness discretization

The solid-shell element presented in [3] is now used to discretize layered structures. One possibility would be to stack up multiple solid-shell elements over each other, i.e. to use one or several elements per layer. But since this is a very expensive approach, we follow a more efficient ansatz by discretizing the entire composite with only one solid-shell over the whole thickness using multiple integration points in that direction representing individual material properties of each layer, cf. Fig. 2. This approach can be understood as a special case of well known equivalent-single-layer theories, e.g. [9, 10], with extension to the geometrical nonlinear regime, as it was already presented in [11]. Since we want to use the Gauss-Legendre quadrature rule within this one-element approach, we need a consistent distribution of integration points within each layer (i.e. subdomain). Therefore we apply a general algorithm for composite materials, similar to [12]. After a first (standard) isoparametric map for the element geometry, see Fig. 3 , we introduce a second isoparametric map for each layer thickness. The thickness coordinate of the first isoparametric space is interpolated as

$$\zeta = \sum_{i=1}^{nlay} \bar{N}_i \, \zeta_i, \quad \text{with} \quad \bar{N}_i = \frac{1}{2}(1 + \bar{z}_i \, \bar{z}) \tag{13}$$

where ζ_i represents the thickness coordinate of the considered layer. In addition the coordinate $-1 \leq \bar{z}_i \leq 1$ is defined within a second isoparametric space, see Fig. 4. In

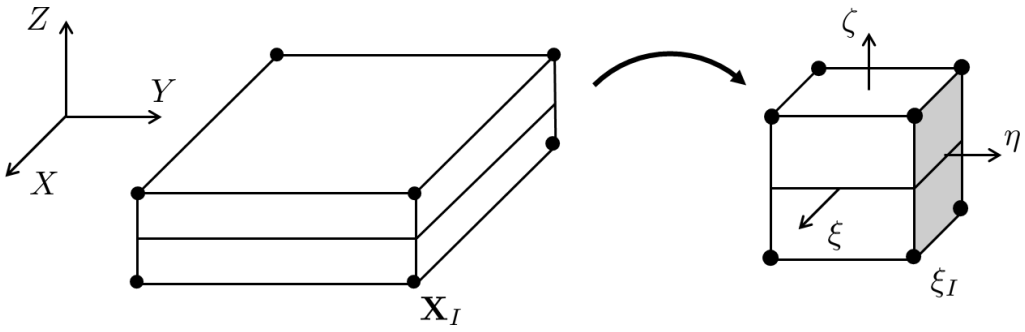

Figure 3: First isoparametric map for the element geometry

order to evaluate the element matrices given in [3] we have to sum over all layers *nlay* and over all integration points *ngp*. For instance the evaluation of the material part of the element stiffness matrix corresponding to the integration points reads:

$$\boldsymbol{K}_{uu}^{\star\,\mathrm{mat}} = 4J^0 \int_{-1}^{1} \boldsymbol{B}_c^{\star\,T}\, \hat{\boldsymbol{C}}^{\star}\, \boldsymbol{B}_c^{\star}\, d\zeta \tag{14}$$

$$\approx 4J^0 \sum_{L=1}^{nlay} \sum_{m=1}^{ngp} \left[\boldsymbol{B}_c^{\star\,T}(\zeta_m^L)\, \hat{\boldsymbol{C}}^{L}\, \boldsymbol{B}_c^{\star}(\zeta_m^L) \right] J^L w_m^L \,, \tag{15}$$

where $\boldsymbol{B}_c^{\star}$ denotes the discrete gradient operator coming from the compatible strain and $\hat{\boldsymbol{C}}^L$ determines the constant stiffness tensor of the considered layer in Voigt-notation. Furthermore J^0 and J^L represent the determinant of the Jacobian matrix of the first and second map, respectively and w_m^L depicts the weighting factor of the considered integration point.

3.2 Adjustment of the hourglass stabilization

The two-field formulation of the enhanced strain method is transferred into an equivalent reduced integration concept by carrying out a Taylor expansion of the stress measure

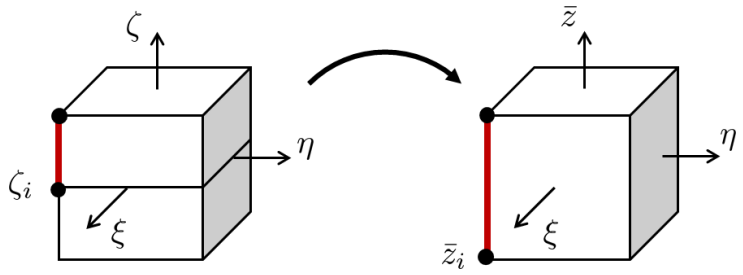

Figure 4: Second isoparametric map for each layer

with respect to the shell director $\boldsymbol{\xi}^\star = (0, 0, \zeta)^T$:

$$\hat{\boldsymbol{S}} \approx \hat{\boldsymbol{S}}\Big|_{\boldsymbol{\xi}=\boldsymbol{\xi}_\star} + \frac{\partial \hat{\boldsymbol{S}}}{\partial \xi}\Big|_{\boldsymbol{\xi}=\boldsymbol{\xi}_\star} (\xi - 0) + \frac{\partial \hat{\boldsymbol{S}}}{\partial \eta}\Big|_{\boldsymbol{\xi}=\boldsymbol{\xi}_\star} (\eta - 0) \tag{16}$$

$$\approx \hat{\boldsymbol{S}}^\star + \hat{\boldsymbol{C}}^\star \, \hat{\boldsymbol{E}}^{hg} \tag{17}$$

With that we are able to split the element residual vectors and further the element stiffness matrices into two parts. A physical relevant part corresponding to the integration points located at the shell director and an hourglass part which stabilizes the element formulation. Therefore, we have to choose an appropriate hourglass stabilization matrix $\hat{\boldsymbol{C}}^\star$ which prevents additional zero eigenvalues of the element stiffness matrix (so-called zero energy modes) coming from the reduced integration. Since we deal with structures consisting of several orthotropic layers, we suggest two different stabilization schemes. First, we introduce a so-called physical stabilization scheme, which is based on the real material stiffness:

$$\hat{\boldsymbol{C}}^\star := \sum_{L=1}^{nlay} (\hat{\boldsymbol{C}}^L)\, w^L \quad \text{with} \quad \hat{\boldsymbol{C}}^L := \frac{\partial^2 \psi^{ud}}{\partial \hat{\boldsymbol{E}} \, \partial \hat{\boldsymbol{E}}} \tag{18}$$

Here we sum over all constant layer stiffnesses $\hat{\boldsymbol{C}}^L$ multiplied with a scalar weighting factor, which fulfils $\sum_{L=1}^{nlay} w^L = 1$ and which depends on the specific layer thickness. Next, we consider a simplified stabilization scheme which is based on a pseudo isotropic material:

$$\hat{\boldsymbol{C}}^\star := 2\mu^\star \boldsymbol{I} \quad \text{with} \quad \mu^\star := \sum_{L=1}^{nlay} \frac{S_{eq}^{\star\, L}}{E_{eq}^{\star\, L}}\, w^L \tag{19}$$

Here we introduce an effective shear modulus $\mu^\star$, which is computed from the quotient of the equivalent stress and strain evaluated at the integration points, multiplied with the thickness weighting factor, which was already introduced in (18). Furthermore, $\boldsymbol{I}$ represents the identity matrix. A similar stabilization scheme was first introduced by [13] and further investigated by [3] for isotropic materials, in order to take into account the degree of inelasticity within the hourglass stabilization.

4 NUMERICAL EXAMPLE

As an example we consider a pinched half-cylindrical shell. Fig. 5 shows a sketch of the geometry with boundary conditions and loading. The dimensions of the cylinder are given by the length $l = 304.8$, inner radius $r = 100.1$ and thickness $t = 3.0$. For this structure we consider three different material configurations. An isotropic one with Young's modulus $E = 2.0685 \cdot 10^7$ and Poisson's ratio $\nu = 0.3$ as well as two anisotropic configurations consisting of three layers with equal thicknesses and the stacking sequences $[0°/90°/0°]$ and $[90°/0°/90°]$, respectively. The values of the engineering constants, taken from [14] and the equivalent model parameters for the anisotropic case are listed in Table 1. The

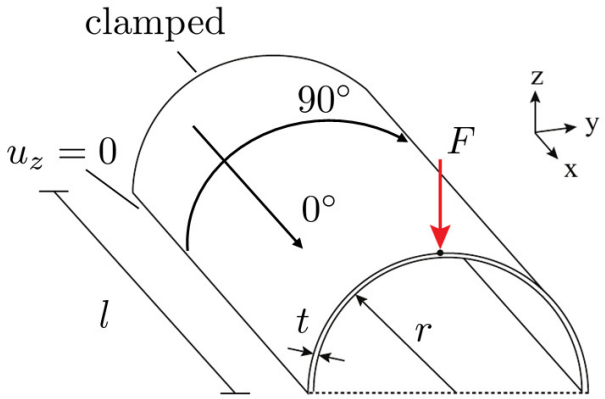

Figure 5: Sketch of the pinched half cylinder problem

Table 1: Engineering constants and equivalent material parameters for the anisotropic configurations

E_1	=	2068.50	K_1^{iso}	=	74.21
E_2	=	517.13	K_2^{iso}	=	−99.45
G_{12}	=	795.60	K_1^{ani}	=	−106.48
G_{23}	=	198.89	K_2^{ani}	=	298.35
ν_{12}	=	0.30	K^c	=	10.25

load is applied incrementally up to $F = 1400$. For the quadrature in thickness direction we used two Gauss-points per layer. Furthermore we carried out a mesh convergence study with respect to the hourglass-stabilization schemes presented in section 3.2 by using the vertical displacement of the load application point. Since we didn't observe a significant influence on the stabilization scheme for the considered configurations in this example, we choose the simplified (isotropic) scheme. Fig. 6 shows the converged undeformed mesh used for all configurations as well as the deformed isotropic mesh after the last load step. The resulting load displacement curves for the considered configurations are depicted in Fig. 7. We can observe an excellent agreement between the present results and the reference solutions from Sze et al. [14], where they used four-node shell elements with reduced integration (S4R) within the commercial FEA software ABAQUS.

5 CONCLUSION

In this paper a specific FE-model was presented in order to determine the global response of layered anisotropic structures. Based on former works, a modified strain energy function was derived which is suitable for a wide range of unidirectional materials. The spatial discretization of layered structures is performed by using one single reduced integration-based solid-shell element over the thickness with multiple integration points. To this end a second mapping procedure as well as a suitable hourglass stabilization scheme were proposed. It should be stated, however, that the suggested stabilization

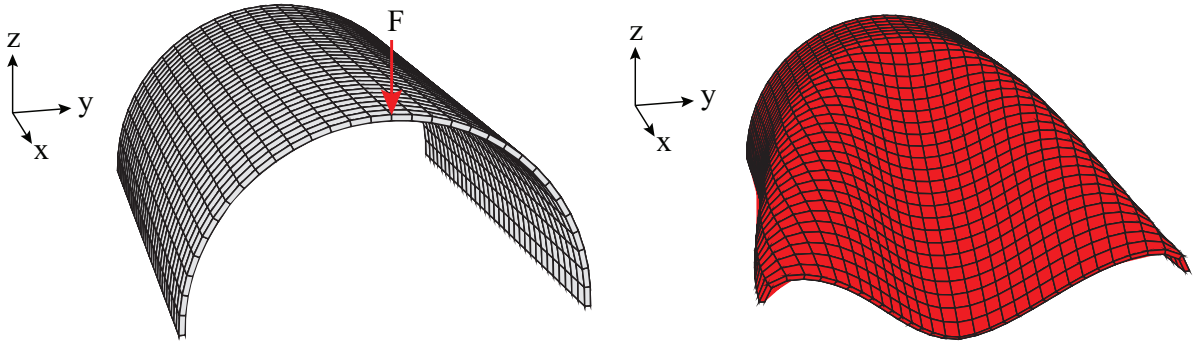

(a) Undeformed configuration

(b) Deformed isotropic configuration

Figure 6: Converged meshes of the half-cylindrical shell

schemes are still under investigation and therefore, not discussed in detail within this paper. A numerical benchmark problem was considered and the underlying concept showed promising results by means of the global response of layered anisotropic shell structures.

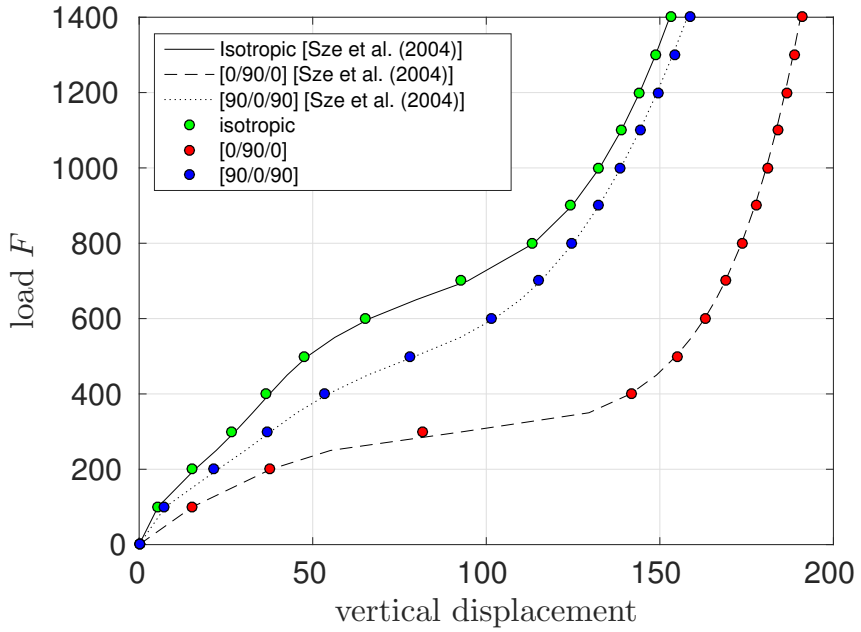

Figure 7: Load displacement curves of the half cylinder for three different configurations

Acknowledgements: Financial support of Subproject D3 of the Transregional Collaborative Research Center SFB/TRR 40 by the German Science Foundation (DFG) is gratefully acknowledged.

REFERENCES

[1] S. Reese, International Journal for Numerical Methods in Engineering **69**, pp. 1671–1716, 2007.

[2] M. Schwarze, S. Reese, International Journal for Numerical Methods in Engineering **80**, 1322–1355, 2009.

[3] M. Schwarze, S. Reese, International Journal for Numerical Methods in Engineering **85**, pp. 289–329, 2011.

[4] J. Frischkorn, S. Reese, Computer Methods in Applied Mechanics and Engineering **265**, pp. 195–212, 2013.

[5] M. Fassin, D. Kowollik, S. Reese, K. Lindhorst and M. Haupt, SFB TRR40 Annual Report 2015 **7**, 239–260, 2015.

[6] F. Breede, S. Hoffmann, N. Jain, R. Jemmali, International Journal of Applied Ceramic Technology **13**, 3–16, 2016.

[7] S. Reese, T. Raible, P. Wriggers, International journal of solids and structures **38**, 9525–9544 2001.

[8] S. Reese, T. Raible, P. Wriggers, International journal of solids and structures **40**, 951–980 2003.

[9] J. N. Reddy, CRC press, 2004.

[10] E. Carrera, Archives of Computational Methods in Engineering, **10**, 215–296 2004.

[11] O. Barfusz, S. Reese, Proceedings in Applied Mathematics and Mechanics, **17**, 397–398, 2017.

[12] S. Klinkel, F. Gruttmann, W. Wagner, Computers & Structures **71**, 43–62 1999.

[13] T. Belytschko, L.P. Bindeman, Computer Methods in Applied Mechanics and Engineering **105**, 225–260 1993.

[14] K.Y. Sze, Finite elements in analysis and design **40**, 1551–1569 2004.